Electronic Supplementary Information

Upcycling of plastic waste into carbon nanotubes as efficient battery additives

Eonu Nam,‡[a] Gyori Park,‡[b] Ji Young Nam,[c] Sooryun Park,[d] Yoonjeong Jo,[a] Jihun Kim,[a] Byung Gwan Park,[a] Kyungeun Baek,[a] Seok Ju Kang,[a] Ho Won Ra,[c] Youngsoo Park,[d] Myung Won Seo,*[e] Kyung Jin Lee*[b], and Kwangjin An*[a]

[a]School of Energy and Chemical Engineering, and Graduate School of Carbon Neutrality, Ulsan National Institute of Science and Technology (UNIST), Ulsan 44919, Republic of Korea.

[b]Department of Chemical Engineering and Applied Chemistry, Chungnam National University, Daejeon 34134, Republic of Korea.

[c]Climate Change Research Division, Korea Institute of Energy Research (KIER), Daejeon 34129, Republic of Korea

[d]Korea Carbon Industry Promotion Agency, Jeonju 54853, Republic of Korea

[e]School of Environmental Engineering, University of Seoul, Seoul 02504, Republic of Korea.

‡These authors contributed equally to this work.

*To whom correspondence should be addressed (E-mail: kjan@unist.ac.kr)

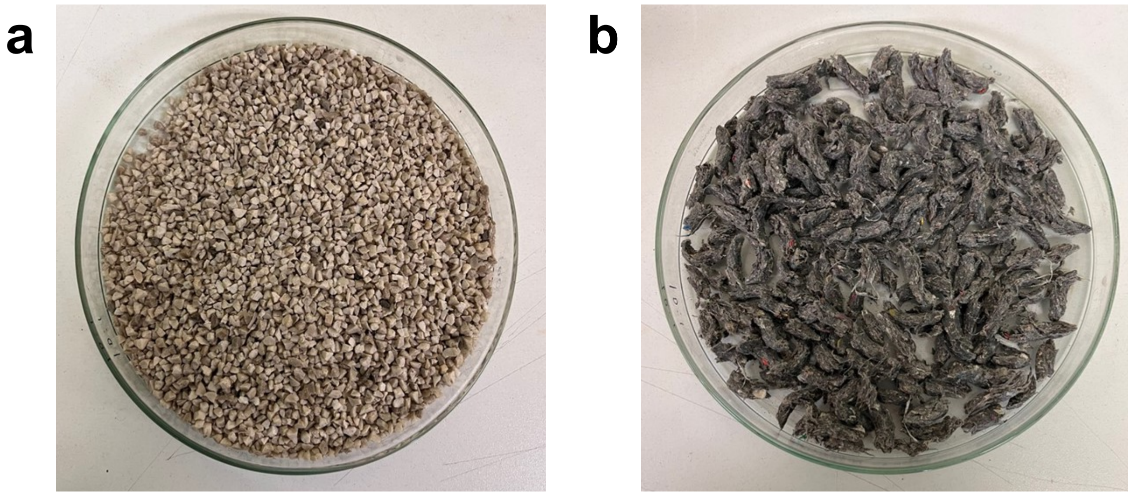

Fig. S1. Photographs of (a) masks and (b) SRF pellets used in pyrolysis.

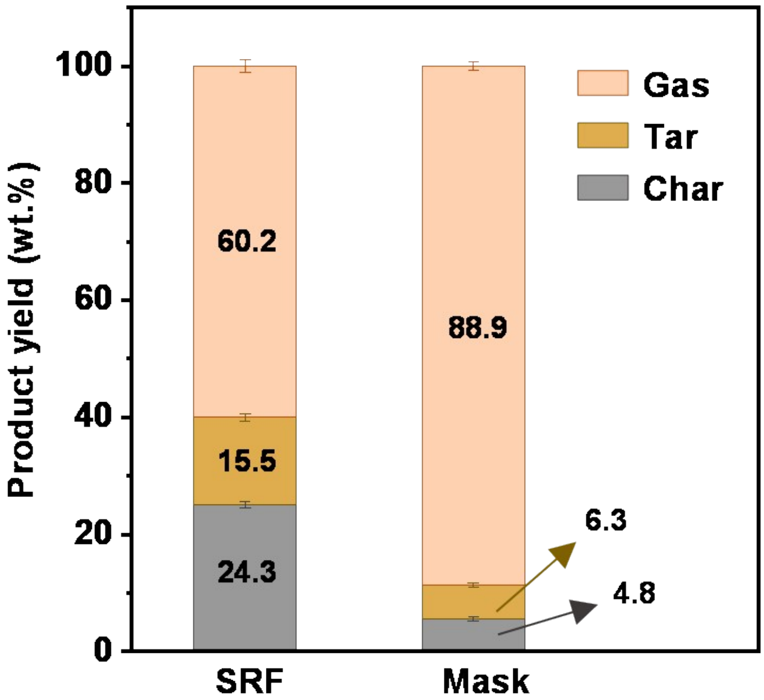

Fig. S2. Product yields of SRF and mask waste after pyrolysis at 800 °C.

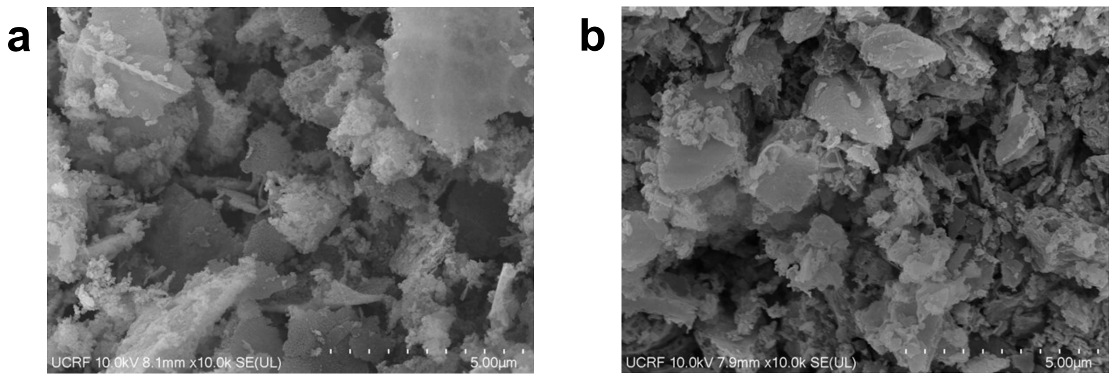

Fig. S3. SEM images of the as-prepared (a) CoMo/MgO and (b) FeMo/MgO catalysts.

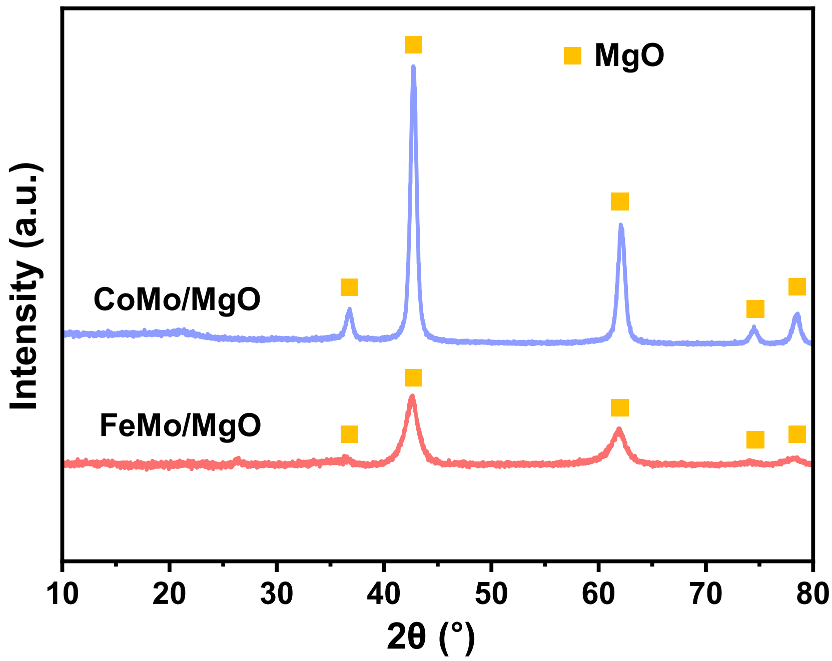

Fig. S4. XRD patterns of the as-prepared CoMo/MgO and FeMo/MgO catalysts.

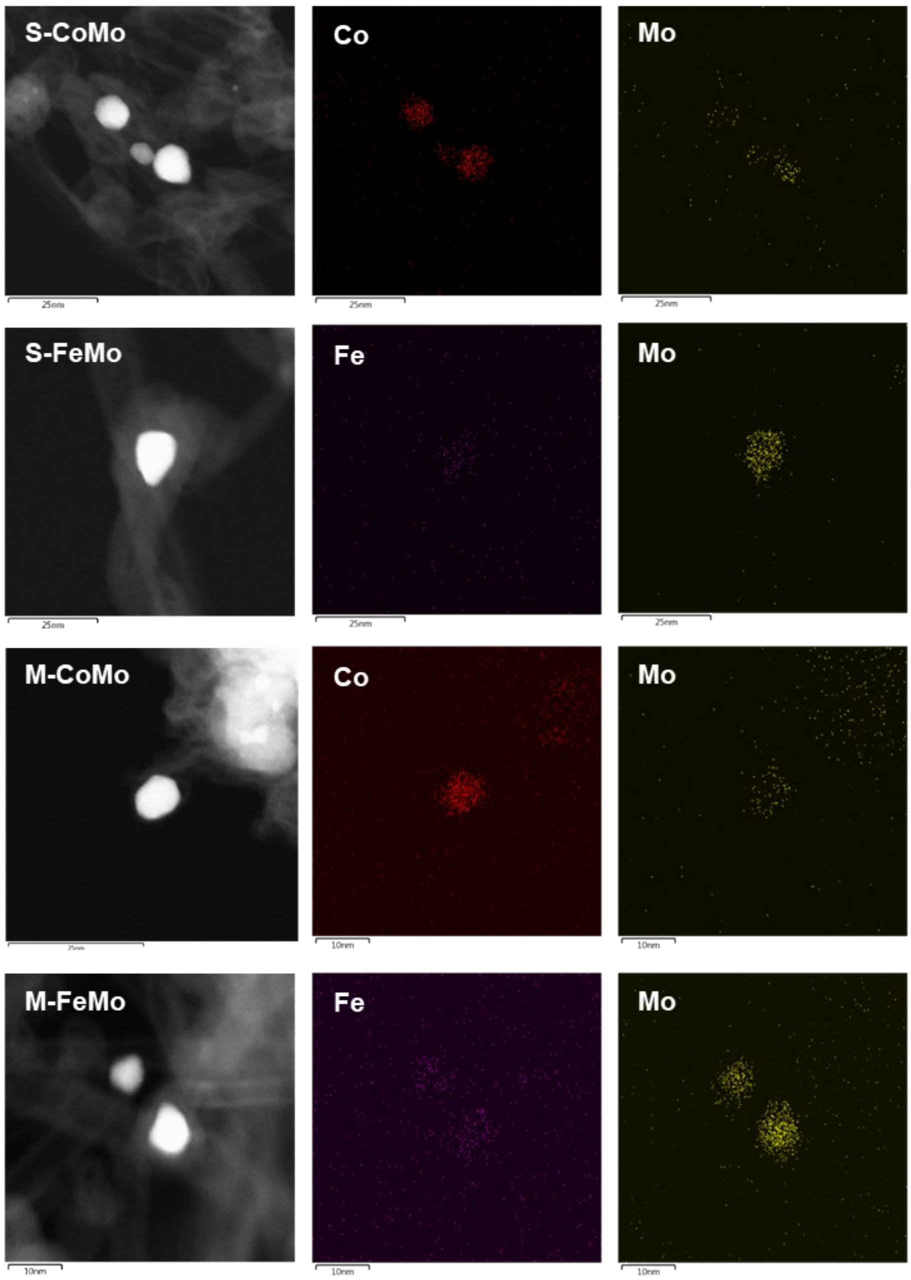

Fig. S5. HAADF-STEM and EDS mapping images of the spent catalysts (S-CoMo, S-FeMo, M-CoMo, and M-FeMo) after CVD.

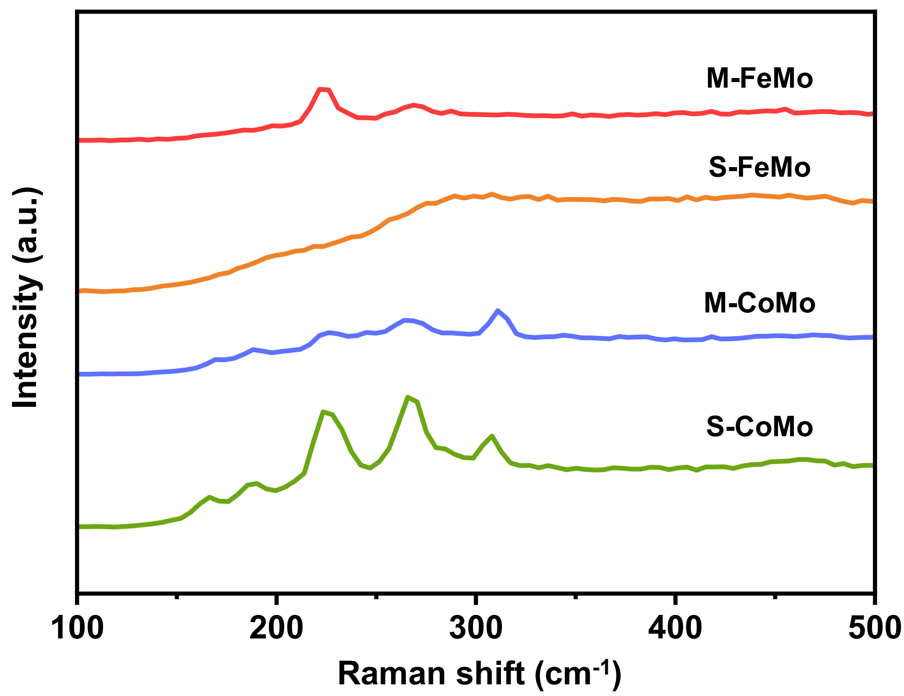

Fig. S6. Low-frequency Raman spectra of the plastic-derived CNTs on the spent catalysts.

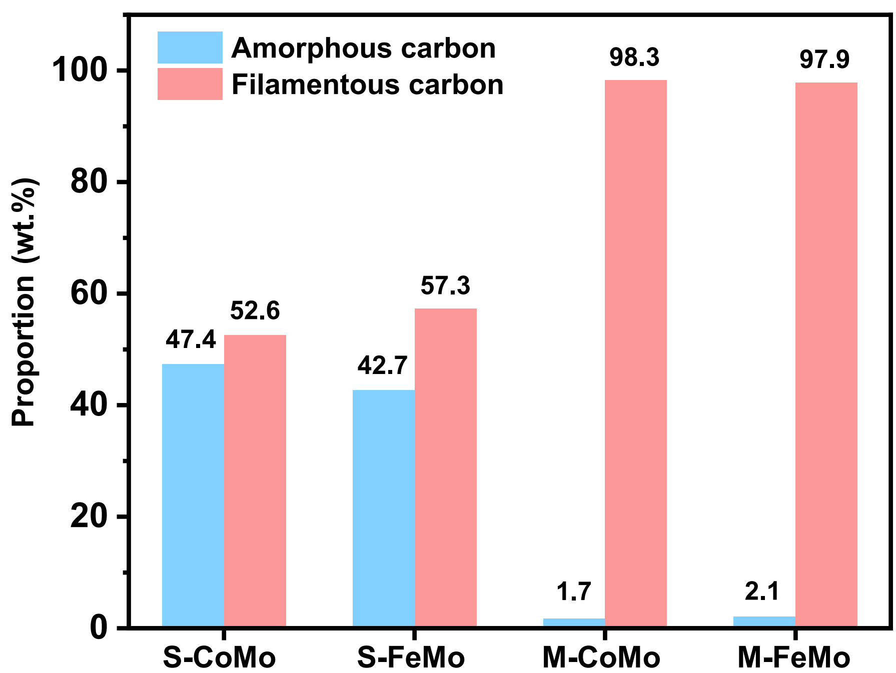

Fig. S7. Mass ratios of amorphous carbon and filamentous carbon in the spent catalysts calculated using the TPO and derivative TPO profiles.

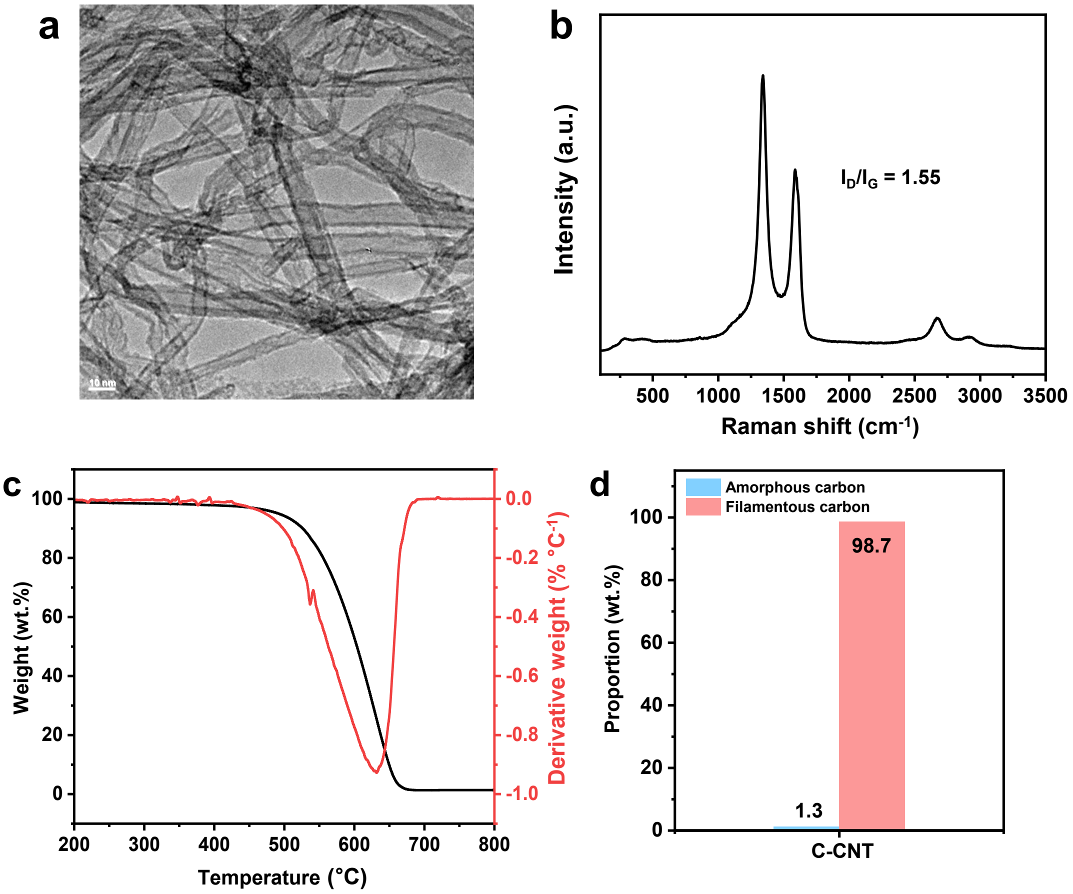

Fig. S8. (a) TEM image, (b) Raman spectrum, (c) TPO and derivative TPO profiles, and (d) mass ratios of the amorphous and filamentous carbon in commercial CNTs (C-CNTs).

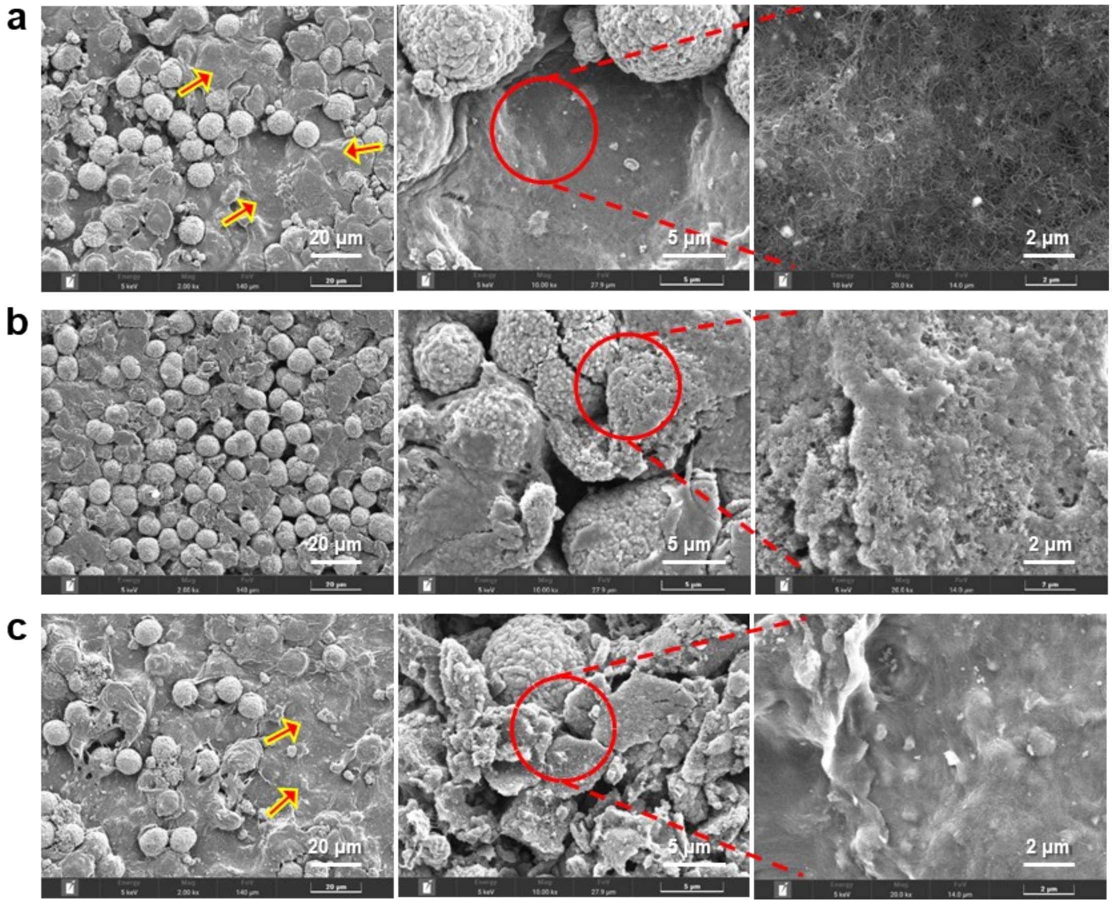

Fig. S9. SEM images of the electrode surfaces with the different types of CNTs: (a) C-CNT, (b) FeMo-CNT, and (c) CoMo-CNT.

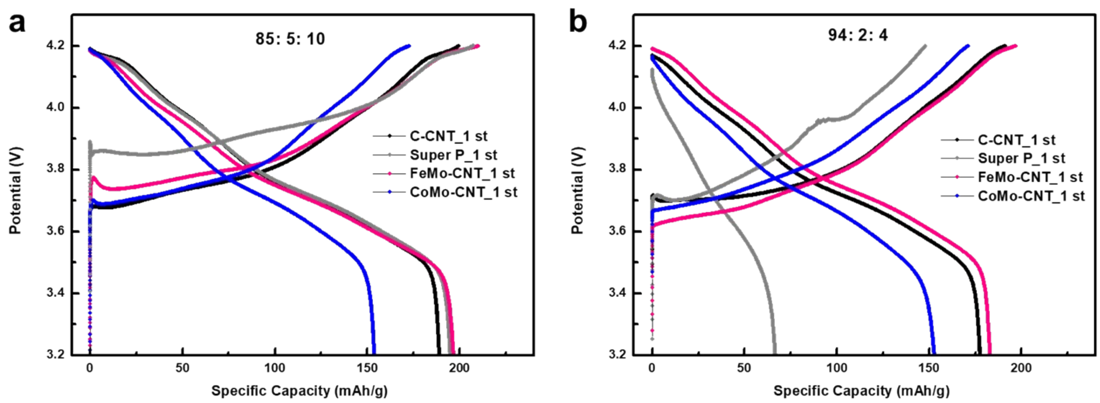

Fig. S10. First discharge-charge profiles at 0.1 C of each electrode at ratios of (a) 85 : 5 : 10 and (b) 94 : 2 : 4.

Table S1. Results of the ultimate and proximate analyses of masks and SRF (dry basis).

Feedstock	Ultimate analysis (wt.%)						Proximate analysis (wt.%)			
	C	H	O[a]	N	S	Cl	Volatiles	Moisture	Ash	Fixed carbon
Masks	79.1–80.7	12.2–12.4	5.8–7.3	0.5–0.7	0	0	87.2–88.8	0.3–0.5	0.5–0.8	10.4–11.0
SRF	57.9–61.4	7.3–8.0	21.5–24.8	0.2–0.3	0–0.1	0.3–0.5	81.0–84.3	4.1–4.6	8.6–9.2	3.7–4.0

[a]Calculated as [O] = 100% –{[C]+[H]+[N]+[S]+[ash]}.

Table S2. Composition of gas (vol.%) obtained by pyrolysis of the mask waste and SRF.

Components	Mask gas	SRF gas
CH_4	4.62–4.63	1.76–1.79
C_2H_4	4.04–4.07	1.47–1.51
C_2H_2	0.09–0.10	0.08
C_2H_6	0.33–0.35	0.11
C_3H_6 (Propylene)	0.84–0.89	0.20–0.22
C_3H_8	0.02	-
C_3H_4 (Propadiene)	0.03	0.01
C_3H_4 (Propyne)	0.05	0.01
i-C_4H_8	0.12	0.02
C_4H_8 (1-Butene)	0.21	0.06
C_4H_8 (trans-2-butene)	0.01	-
C_5H_{10} (1-pentene)	0.08–0.09	0.02
C_5H_{10} (2-methyl-2-butene)	0.03–0.04	0.01
H_2	2.28–2.29	1.31–1.56
CO	0.96–0.97	1.68–1.73
CO_2	0.52	1.12–1.14
N_2	85.65–85.73	91.83–92.11

Table S3. Results of elemental analysis using SEM-EDS, surface area, and pore volumes of the as-prepared CoMo/MgO and FeMo/MgO catalysts.

Catalyst	SEM-EDS			S_{BET} (m^2 g^{-1})	Pore volume (cm^3 g^{-1})
	Co (wt.%)	Fe (wt.%)	Mo (wt.%)		
CoMo/MgO	8.8	-	2.9	37.9	0.351
FeMo/MgO	-	2.7	21.1	27.1	0.209

Table S4. Effect of catalysts on the composition of pyrolysis gas (vol.%) generated from masks (denoted as "Mask" or "M-") and SRF (denoted as "SRF" or "S") on N_2-free basis. After CVD was conducted, the type of catalyst (CoMo or FeMo) is given after the hyphen.

Components	Mask	M-CoMo	M-FeMo	SRF	S-CoMo	S-FeMo
CH_4	32.28–32.36	32.82–33.10	17.17–17.47	21.58–22.25	21.66–22.06	17.21–18.10
C_2H_4	28.34–28.38	8.14–8.20	0.50–0.54	18.03–18.83	7.92–8.07	3.95–4.13
C_2H_2	0.61–0.67	1.40–1.42	0.01–0.02	0.92–0.98	1.49–1.50	0.09–0.12
C_2H_6	2.29–2.31	0.24–0.26	0.06–0.07	1.35–1.41	0.08–0.10	0.07–0.08
C_3H_6 (Propylene)	6.04–6.08	0.07–0.08	-	2.52–2.63	0.05	0.02
C_3H_8	0.13–0.14	-	-	0.05–0.06	-	-
C_3H_4 (Propadiene)	0.20	0.01	-	0.08–0.09	0.01	-
C_3H_4 (Propyne)	0.35–0.37	0.02	-	0.15–0.16	0.01–0.02	-
i-C_4H_8	0.79–0.82	-	-	0.19–0.20	-	-
C_4H_8 (1-Butene)	1.44–1.46	0.08–0.09	-	0.77–0.81	0.07–0.08	0.02–0.03
C_4H_8 (trans-2-Butene)	0.03–0.04	-	-	0.02	-	-
C_5H_{10} (1-Pentene)	0.58–0.61	0.01–0.02	-	0.27–0.29	-	-
C_5H_{10} (2-Methyl-2-butene)	0.23–0.25	-	-	0.08–0.09	-	-
H_2	15.93–16.04	45.50–46.52	69.83–70.31	16.56–19.06	35.58–36.81	40.63–42.53
CO	6.70–6.73	7.96–7.99	11.09–11.26	20.97–21.48	23.78–25.52	34.26–35.08
CO_2	3.61–3.68	2.70–3.33	0.79–0.87	13.92–14.24	7.51–7.55	1.84–1.85

Table S5. Characteristics of the mask-derived and commercial CNTs and commercial carbon black.

Sample	Average diameter (nm)	I_D/I_G ratio	CNT purity (%)	Surface area ($m^2\ g^{-1}$)
FeMo-CNT	5.4	0.28	97.9	271.0
CoMo-CNT	3.5	0.27	98.3	207.4
C-CNT	6.1	1.55	98.7	246.8
Super P	-	-	-	63.3

[a]I_D represents the intensity of the D-band in the Raman spectrum.

[b]I_G represents the intensity of the G-band in the Raman spectrum.

Table S6. First discharge-charge capacity and initial coulombic efficiency (ICE) of the 85 : 5 : 10 electrodes with different carbon materials.

	First charge capacity ($mAh\ g^{-1}$)	First discharge capacity ($mAh\ g^{-1}$)	ICE (%)
C-CNT	199.7	189.6	94.9
Super P	207.3	195.7	94.4
FeMo-CNT	210.2	197.6	94.0
CoMo-CNT	172.8	154.5	89.4

Table S7. First discharge-charge capacity and ICE of the 94 : 2 : 4 electrodes with different carbon materials.

	First charge capacity ($mAh\ g^{-1}$)	First discharge capacity ($mAh\ g^{-1}$)	ICE (%)
C-CNT	191.4	178.8	93.4
Super P	148.0	67.5	45.6
FeMo-CNT	196.9	184.2	93.6
CoMo-CNT	171.2	153.9	89.9